Biophysical Journal
Article

Biophysical Society

Single-Molecule Chemo-Mechanical Spectroscopy Provides Structural Identity of Folding Intermediates

Hesam N. Motlagh,[1,*] Dmitri Toptygin,[2] Christian M. Kaiser,[2] and Vincent J. Hilser[1,2,*]
[1]T.C. Jenkins Department of Biophysics and [2]Department of Biology, The Johns Hopkins University, Baltimore, Maryland

ABSTRACT Single-molecule force spectroscopy has emerged as a powerful tool for studying the folding of biological macromolecules. Mechanical manipulation has revealed a wealth of mechanistic information on transient and intermediate states. To date, the majority of state assignment of intermediates has relied on empirical demarcation. However, performing such experiments in the presence of different osmolytes provides an alternative approach that reports on the structural properties of intermediates. Here, we analyze the folding and unfolding of T4 lysozyme with optical tweezers under a chemo-mechanical perturbation by adding osmolytes. We find that two unrelated protective osmolytes, sorbitol and trimethylamine-*n*-oxide, function by marginally decelerating unfolding rates and specifically modulating early events in the folding process, stabilizing formation of an on-pathway intermediate. The chemo-mechanical perturbation provides access to two independent metrics of the relevant states during folding trajectories, the contour length, and the solvent-accessible surface area. We demonstrate that the dependence of the population of the intermediate in different osmolytes, in conjunction with its measured contour length, provides the ability to discriminate between potential structural models of intermediate states. Our study represents a general strategy that may be employed in the structural modeling of equilibrium intermediate states observed in single-molecule experiments.

INTRODUCTION

Single-molecule force spectroscopy has emerged as a powerful tool for studying protein folding (1–3). Devoid of ensemble averaging, mechanical manipulation of single protein molecules with optical tweezers has revealed a wealth of mechanistic information on transient states and intermediates that would otherwise have been obscured in ensemble measurements (1–11). To date, state assignment of these intermediates and structural transitions has relied on changes in contour length and empirical domain boundary demarcation (7,9–11). Only recently, studies have begun to identify structural intermediates through mutational analysis (6), although such experiments are time-consuming, difficult, and not applicable to all systems. Performing force spectroscopy experiments in the presence of osmolytes, however, represents an alternative approach, providing a chemo-mechanical perturbation that reports on the relative accessible surface area (ASA) of states in addition to contour length (2,12–15).

Protective osmolytes are ubiquitous small organic molecules that have evolved in nature to counteract the deleterious effects of harsh environmental conditions experienced by many organisms (16). In elasmobranchs, for example, up to 0.4 M urea can accumulate in the cytosol, introducing significant denaturing stresses to the proteins in the cytosolic milieu (16). Protective osmolytes function by stabilizing folded conformations of proteins, and despite the fact that osmolytes fall into different chemical classes (e.g., polyols and methylamines), and that different osmolytes interact to different extents with the protein backbone and side chains, the overall effect of stabilizing folded conformations relative to unfolded conformations appears similar (12,15).

Despite the fact that the impact of osmolytes on protein stability can be accurately predicted from surface area changes (12–16), a mechanistic understanding of how osmolytes modulate the energy landscape of proteins (known as the osmophobic effect) remains elusive. In particular, it is clear from ensemble measurements that osmolytes affect both folding and unfolding kinetics (17–20), yet mechanistic information on how they change the folding pathway is lacking. Although single-molecule studies with atomic force microscopy (AFM) have revealed that in high concentrations of osmolyte, the unfolding kinetics are slowed and compaction of unfolded species occurs faster when force is quenched (21–24), those studies were performed in a force regime that did not permit direct observation of folding.

Submitted September 2, 2015, and accepted for publication December 31, 2015.

*Correspondence: hilser@jhu.edu or hnekoor1@jhu.edu

Editor: James Cole.
http://dx.doi.org/10.1016/j.bpj.2015.12.042

To address these limitations and to determine whether the known transfer free energy correlations (12–14) could be leveraged into single-molecule experiments, we performed single-molecule force spectroscopy on the cysteine-free variant of T4 lysozyme [T4*] (25) in different osmolytes using optical tweezers. T4* consists of two coupled subdomains; a sequentially contiguous N-terminal domain and a sequentially discontiguous C-terminal domain (Fig. 1 *a*). T4* has been extensively studied both at the ensemble (26,27) and at the single-molecule level (5,7), and is known to fold through an intermediate state. As such, it is an ideal system to perturb with osmolyte to characterize both the unfolded to intermediate, as well as the intermediate to native state transitions.

We conducted single-molecule experiments in the absence and the presence of two different osmolytes, sorbitol and TMAO (trimethylamine *n*-oxide), representing two different classes of osmolyte molecules (Fig. 1 *b* and Materials and Methods for details). Their impact on the mechanical unfolding and refolding rates was determined. Because our single-molecule force spectroscopy experiments provide the extension change as well as the different osmolyte sensitivities of the intermediate state population, we are able to reliably determine the structural properties of the intermediate state. In addition, we show that we are able to discriminate between multiple detailed structural models of the intermediate. The resultant approach may represent a general strategy for characterizing structures populated during protein folding, thereby adding to the library of information that can be gleaned from single-molecule experiments.

MATERIALS AND METHODS

Pulling buffers and materials

All pulling experiments were conducted in buffer HKM (25 mM HEPES*KOH, 150 mM KCl, 5 mM $MgCl_2$, pH 7.4). TMAO (trimethylamine *n*-oxide dehydrate) was purchased from Sigma-Aldrich (St. Louis, MO) and dissolved with the components of pulling buffer. To remove impurities from TMAO synthesis, all buffers were stirred with activated carbon (12-20 mesh; Sigma-Aldrich) for 1 h while protected from light. Sorbitol was purchased from Sigma-Aldrich. The buffers were filtered (0.22 μm filter; Millipore, Billerica, MA), divided into aliquots, and stored at −80°C until use. All beads were purchased from Spherotech (Lake Forest, IL).

Protein purification

The plasmid harboring the single-molecule cysteine-free variant of T4 Lysozyme (T4*) was provided from Kaiser et al. (7). The construct contains an N-terminal Avi Tag for biotinylation (28), a flexible linker, the open reading frame of T4*, and then a YbbR tag on the C-terminus for addition of Coenzyme A (CoA) cross-linked to oligonucleotide (29). The insert was subcloned into a pET vector with a 9X-His-Tag and a TEV protease site adjacent to the Avi-tag used for biotinylation. The plasmid was transformed into Rosetta 2(DE3)pLysS (EMD Millipore) and plated on LB plates with 100 μg/mL ampicillin. The next day colonies were picked and grown to preparative volumes at 37°C 250 rpm until the OD_{600nm} reached 0.6–0.8. Expression was induced with 1 mM IPTG under the same conditions for 3 h. Cells were harvested by centrifugation and stored at −80°C. Pellets were resuspended in Lysis Buffer (50 mM NaH_2PO_4, 300 mM NaCl, 20 mM Imidazole, pH 8.0) and lysed by five passes through an EmulsiFlex C3 (Avestin, Ottawa, Ontario, Canada) at 15,000 psi. Lysates were clarified by centrifugation and immediately loaded onto HisPur Ni-NTA Superflow Agarose (Thermo Scientific, Waltham, MA) and eluted with a linear gradient with the same buffer containing 500 mM imidazole. Samples containing T4* were pooled and dialyzed to TEV digestion buffer (50 mM Tris-HCl, 0.5 mM EDTA, 1 mM DTT, pH 8.0) along with TEV protease (1 μM final concentration). Cleaved T4* was recovered by running through the same nickel affinity resin, dialyzed to 1× PBS, concentrated to 100 μM, and flash-frozen with liquid nitrogen. It should be noted that the single-molecule data collected indicate that T4* is in its native state and unperturbed from the modification tags. This is indicated by the molecule folding cooperatively and reproducibly to a state that is not only consistent in dimensions to the native state, but also demonstrates reproducible kinetics of unfolding as previously demonstrated in Kaiser et al. (7).

Synthesis of oligonucleotide cross-linked to CoA

OligoCoA (oligonucleotide cross-linked to CoA) was synthesized as previously described in Kaiser et al. (7) and Maillard et al. (8) except OligoCoA was purified by reverse-phase high-performance liquid chromatography. After cross linking, samples were isopropanol-precipitated and resuspended in Milli-Q water (Millipore). The samples were then desalted by an illustra MicroSpin G-25 Column (GE Healthcare, Port Washington, NY) according to the manufacturer's instructions. Samples were concentrated by vacuum centrifugation and then purified by semipreparative reverse-phase high-performance liquid chromatography on an 1100 Series instrument (Agilent Technologies, Santa Clara, CA). Modified oligonucleotide was separated using a 250 × 10 mm Jupiter C18 column (Phenomenex, Torrance, CA) packed with 5 μm particles. Mobile phase A was 100 mM TEAA (triethylammonium acetate) pH 7.0, and mobile phase B was the same except

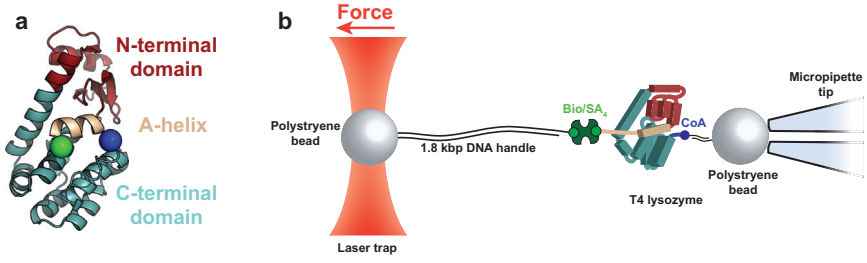

FIGURE 1 T4 Lysozyme as a model system and single-molecule folding experimental setup. (*a*) Cartoon representation of T4 Lysozyme (PDB: 2LZM). Highlighted is the N-terminal A-helix (*beige*, residues 1–11), the N-terminal subdomain (*red*, residues 12–66), and the C-terminal subdomain (*cyan*, resides 67–164). Also shown are the attachment points for single-molecule force spectroscopy experiments (*green* and *blue spheres*). (*b*) In the experimental setup, a polystyrene bead is held in the trap that exerts force on the single molecule. The bead is covalently linked to 1.8 kbp of dsDNA, which is attached to biotin (*green circle*) at the other end. There is a noncovalent biotin/streptavidin interaction that then is linked to T4. CoA (*blue circle*) is covalently linked to T4 and another 50 bp of dsDNA that is attached to the polystyrene bead, which is held by suction. To see this figure in color, go online.

with the addition of 15% acetonitrile. The column was equilibrated to 60°C and samples were eluted by a linear gradient of 0–100% B over 30 min and then holding 100% B for another 30 min while detecting absorption at 260 nm. Pure fractions were confirmed by urea-polyacrylamide gel electrophoresis. Samples were finally isopropanol-precipitated and confirmed by matrix-assisted laser desorption/ionization time-of-flight mass spectrometry.

Labeling of protein for optical tweezer experiments

The labeling occurred in two major steps: a biotinylation reaction specific to the N-terminus followed by attachment of CoA (that was cross linked to double-stranded oligonucleotide) to the C-terminus. Before the optical tweezer experiments, modified protein molecules were ligated directly to polystyrene beads. During experiments, tethers were generated via a noncovalent biotin/streptavidin/biotin interaction in situ (i.e., in the microfluidics chamber) between the N-terminal biotin and the streptavidin/biotin complex on the surface of the DNA bead held in the trap (see below). Many of these methods are previously described in Kaiser et al. (7) and Maillard et al. (8), and modifications to these protocols are described for completeness.

The T4* construct harbored an N-terminal Avi tag sequence (GLNDIFEAQKIEWHE) that is specifically modified by *Escherichia coli* biotin ligase (BirA) at lysine 10 in the sequence (28). BirA was purified as previously described in Kaiser et al. (7). Purified protein was mixed with 1× biotinylation buffer (20× = 500 μM D-biotin, 100 mM ATP, 100 mM Mg(OAc)), 2 μM BirA, and allowed to react for 2 h at room temperature. Samples were then dialyzed against 1× PBS to remove excess biotin. Biotinylated protein was purified by using Pierce Monomeric Avidin Resin (Thermo Scientific) according to manufacturer's instructions. Samples containing biotinylated protein were dialyzed to 1× PBS.

The T4* construct also harbored a C-terminal YbbR tag (DSLEFIASKLA), which is specifically modified at serine 2 by the phosphopantethein moiety of CoA in an enzymatic reaction catalyzed by the phosphopantethein transferase Sfp from *Bacillus subtilis* (30). Sfp was prepared as previously described in Yin et al. (29). OligoCoA was annealed to a complimentary strand that had a 4-bp overhang allowing for downstream annealing and ligation of protein to beads. Biotinylated T4* (25 μM) was labeled by mixing freshly annealed dsOligo-CoA (50 μM), Sfp (10 μM), and 1× HM buffer (5× = 50 mM HEPES*KOH, 10 mm $MgCl_2$, pH 7.5) and incubating for 2 h at 37°C. Modification was confirmed by mobility shift in sodium dodecyl sulfate-polyacrylamide gel electrophoresis and unused dsOligo-CoA and Sfp were removed via Pierce Monomeric Avidin Resin (Thermo Scientific). Samples were then dialyzed to 1× PBS overnight, diluted to 5 μM, and flash-frozen with liquid nitrogen.

Synthesis of DNA handles

DNA handles were generated by cross linking a 5′-primer to polystyrene beads (31) and directly amplifying the handle on the bead in a PCR-like fashion. The DNA handle was ~1.8 kbp with ~50% GC content and was amplified from the λ-phage genome. Carboxylic acid coated polystyrene beads (2.8 μm diameter) were spun down and washed in 100 mM MES pH 6.0 multiple times to remove any residual material from manufacturing. The carboxyl groups on the beads were then activated with 40 μg/μL fresh EDC (1-Ethyl-3-[3-dimethylaminopropyl]carbodiimide hydrochloride) three times for a 15-min incubation period. Beads were then quickly washed in 50 mM HEPES pH 7.5 and excess 5′-primer was added (5′-NH_2-ACTGATGCAACTGACTCAGC-3′). The reaction was gently shaken at room temperature for 2 h before quenching via addition of 1 M Tris, pH 7.5 to a final concentration of 10 mM. The beads were then washed extensively with Milli-Q water (Millipore) to remove any unreacted product. The beads were finally spun down and resuspended in an equal volume of 5 mg/mL casein (Affymetrix, Santa Clara, CA) and 1% TWEEN-20 to prevent bead aggregation. The beads were treated as a 5′-primer in a PCR reaction with a 3′-primer harboring a biotin moiety on its 5′-end (5′-bio-GAAAGA ATGGGCATGAGC-3′) as previously described in Kaiser et al. (7). After PCR, the beads were spun down and washed extensively using TE Buffer with 20% glycerol and then finally flash-frozen with liquid nitrogen and stored at −80°C. For optical tweezer measurements, beads were thawed and incubated with streptavidin before dilution and injection into the microfluidics chamber. This protocol yielded stable tethers for multiple rounds of pulling and relaxing up to the overstretching transition at 65 pN (32).

Synthesis of beads for protein ligation

Beads were synthesized as previously described in Kaiser et al. (7) except different primers were used. The two primers used were 5′-NH_2-CATGCGTCCTGATGTTAGCTCTCCG-3′ and 5′-CGCACGGAGAGCTA ACATCAGGACGCATG-3′, which leaves a 4-bp overhang complementary to the OligoCoA/protein.

Optical tweezers measurements and analysis

The optical MiniTweezers system was built and calibrated according to directions available online (http://tweezerslab.unipr.it/). The instrument has a counterpropagating, dual-laser beam single-trap that measures force directly by the change in light momentum (33). Experiments were conducted in a microfluidics chamber with a micropipette tip that was purchased from Steve B. Smith Engineering (Los Lunas, NM). Beads ligated with protein were trapped, moved to a micropipette tip, and held by suction. Subsequently, a bead with DNA handles and streptavidin was trapped and brought within close physical proximity of the protein bead in the micropipette tip. Tethers were confirmed by exerting force and observing behavior described previously in Kaiser et al. (7). Single-molecules were confirmed by overstretching of DNA handles (34). Force and trap position were recorded at a sampling frequency of 400 Hz for all constant velocity (force ramp) and constant force (force clamp) experiments. The total number of single-molecule tethers generated under each condition was: $N_{\text{Buffer}} = 32$ molecules, $N_{\text{Sorbitol}} = 20$, and $N_{\text{TMAO}} = 24$ molecules. Constant force rates were determined from a significant number of transitions (total transitions: $N_{\text{Buffer}} = 1173$, $N_{\text{Sorbitol}} = 605$, and $N_{\text{TMAO}} = 1237$).

Steered molecular dynamics simulations

All simulations were performed with VMD and NAMD molecular dynamics software package (35) with the CHARMM36 force field (36). Initial structure of T4* was obtained from the Protein Data Bank (PDB: 1L63). Due to the large extension of the fully elongated conformation (~600 Å), explicit solvent was intractable given limited computational resources. All simulations were performed using an implicit solvent model: generalized Born with a cutoff radius of 12 Å and an ion concentration of 0.15 M similar to the optical tweezer experiments. Temperature was controlled using Langevin dynamics (damping coefficient 2/ps) at 300 K. Van der Waals interactions were treated as a Lennard-Jones 6-12 potential calculated using the switch method starting at 13 Å and smoothly cut off at 14 Å. The SHAKE method was used on all hydrogen atoms allowing integration steps of 2 fs expediting simulation time.

After hydrogens were built in, the structure was minimized by conjugate gradient for 1000 steps. The system was then equilibrated for 4 ns. Three random points were selected within a 2 ns window of the end of equilibration and used as different starting points in the subsequent simulations. Steered molecular dynamics (SMD) simulations were performed by fixing the C-terminal Cα and pulling on the N-terminal Cα with a spring constant of 1000 pN/Å and a velocity of 4 m/s. The system was pulled until the approximate contour length of T4* was achieved (~58.1 nm). Three trials

of each of these simulations were performed. Trajectories were analyzed by using the VMD software and subsequent analysis scripts described below for surface area and energy calculations.

Structure-based calculations for the intermediate state

The $\Delta\Delta G$ values for intermediates were calculated based on the group transfer free-energy model, which uses experimentally measured free energies of transfer for every amino-acid side chain and the peptide backbone (12,13). Potential unfolded states used in determining statistics of average ASA were generated by mechanically unfolding T4* in silico (described above). Intermediate states were treated as having the crystal structure conformation for the folded portion and the unfolded conformation for the remainder. The ASA to a 1.4 Å rolling sphere was calculated for all states using a subroutine from the COREX algorithm (37). The change in ASA from unfolded to intermediate was calculated for every possible species (i.e., every possible combination of the N-terminus and C-terminus unfolded). Using these values, it was possible to calculate $\Delta\Delta G$ as follows:

$$\begin{aligned}\Delta\Delta G &= \Delta Gtr, I - \Delta Gtr, U \\ &= -\Big(\sum\nolimits_{i=\text{AA type}}\Big[n_i\Delta g^{o}_{tr,i,sc}\Delta\alpha_i^{\text{SC}}\Big] \\ &\quad + \Delta g^{o}_{tr,\text{BB}}\sum\nolimits_{i=AA\ \text{type}}\big[n_i\Delta\alpha_i^{\text{BB}}\big]\Big),\end{aligned}$$

where n_i is the total number of groups of amino acid (AA) type I, Δg^{o}_{tr} is the free energy of transfer for the side chain (SC) or backbone (BB) from 0 to 1 M sorbitol or TMAO, and $\Delta\alpha_i$ is the fractional change in solvent ASA from the unfolded to the intermediate state (12,13). The $\Delta\alpha_i$ values used in the calculation above were the mean values of those consistent with the unfolded state: i.e., all states that fell in the range $\mu_U \pm \sigma_U = 25.3 \pm 2.0$ nm. Detailed derivation and treatment of intermediate states are described in Text S2 in the Supporting Material.

RESULTS AND DISCUSSION

Osmolytes marginally decelerate unfolding rates

To fully characterize the effect of osmolyte on the energy landscape, we first performed mechanical unfolding experiments. Single molecules of T4*, subjected to continuously increasing force by moving the trap at a constant velocity (i.e., force-ramp experiments), exhibited cooperative unfolding (Fig. 2 *a*). The mean unfolding forces ($\langle F_{\text{unf}}\rangle$) obtained in the presence and absence of osmolytes overlap significantly: $F_{\text{unf,buffer}} = 17.6 \pm 1.9$ pN ($N = 224$), $F_{\text{unf,1M Sorbitol}} = 18.2 \pm 2.1$ pN ($N = 288$), and $F_{\text{unf,1M TMAO}} = 18.2 \pm 2.2$pN ($N = 340$), where the error values are the standard deviation (SD) of the force distributions. To quantitatively evaluate the unfolding from such experiments, several force-ramp data sets were collected and analyzed using a model that converts the force rupture distribution to an intrinsic lifetime and distance to transition state (38) (Fig. 2, *b–d*). The model reveals that the distance to the transition state ($\Delta x^{\ddagger} = \sim 2.7$ nm) does not change appreciably in the presence of either osmolyte and that unfolding rates are marginally decelerated (Text S1 in Supporting Materials and Methods). Given that osmolytes stabilize the native states of proteins, our results are not unexpected, as osmolytes have been shown to decrease unfolding rates both in ensemble experiments (17–19) and at the single-molecule level (21–24). It should be noted that osmolytes primarily act on the denatured state and we would expect a more pronounced effect on the folding pathway from the denatured state (discussed below). Additionally, osmolytes do not appear to impact the wormlike

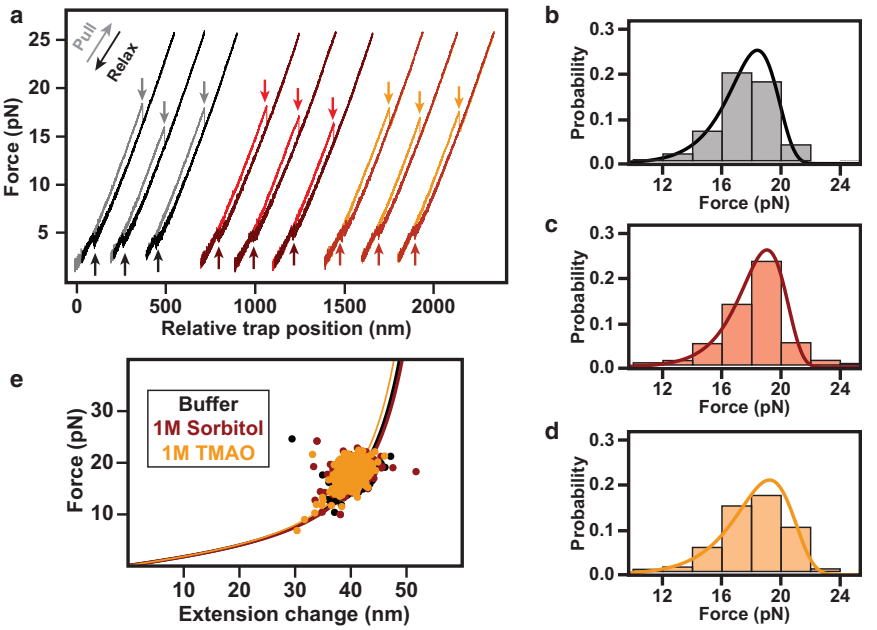

FIGURE 2 The mechanical unfolding pathway is unaffected by osmolyte (*a*). Shown are representative force-extension curves for single molecules of T4 lysozyme generated under constant velocity (100 nm/s). Force-extension curves in buffer (*black*), sorbitol (*red*), and TMAO (*orange*) behave similarly. Unfolding transitions (*lighter arrows pointing down*) were observed in the 12–24 pN regime for all conditions. Refolding occurred in the 3–6 pN regime (*darker arrows pointing up*). (*b–d*) Force rupture probability distributions in the presence of buffer (*black*), sorbitol (*red*), and TMAO (*orange*), respectively. Overlaid on the distributions are the fits using a theoretical model that yields distances to the transition state and lifetimes of the folded state (38). The distributions are well determined and the errors of the fits are smaller than the thickness of the lines. (*e*) Shown are the unfolding transition extension changes (in nanometers) versus the forces of unfolding (in picoNewtons) for every transition observed. Data are color-coded similar to (*a*) and are fit to the wormlike-chain model (55). All contour length changes (ΔL_C) that are consistent with unfolding of the whole molecule are within error of each other. To see this figure in color, go online.

chain model that is used to describe the unfolded state of proteins in force spectroscopy experiments (1,3,7) (Fig. 2 *e*). As a result, we can rule out that osmolytes affect the persistence or contour length in our experiments, at least in the force range covered by the T4* unfolding transitions (~10–20 pN).

To more accurately probe the unfolding landscape, we directly measured unfolding rates in constant-force experiments at different forces. An example trace is shown in Fig. 3 *a*. The molecule initially ($t = 0$) populates the native state and is held at 15 pN until a cooperative unfolding transition occurs. Using data from multiple independent transitions, performed at different forces, we determined the distributions of lifetimes (τ_{app}) at each force, from which we calculated the force-dependent unfolding rate constants ($k_{app,unf}$) (Fig. 3 *b*). Over the experimentally accessible force range, we consistently observed a small yet significant deceleration of T4* unfolding rates in the presence of TMAO and sorbitol consistent with the force-ramp experiments (Fig. 3 *b*).

Using Bell's model (39), we determined the force dependence of the rate constant and the distance to the transition state. The fits with and without osmolyte are not statistically different, yielding zero force unfolding rates (i.e., intercept) within error of each other and $\Delta x^{\ddagger}$ values (i.e., slope) that are comparable to the values obtained from force rupture distributions (Text S1 in Supporting Materials and Methods). This is in apparent contradiction to the force-ramp unfolding rates obtained using a different model. Both models require extrapolation from the unfolding force regime (~15–20 pN) to zero force. As such, both models are subject to error propagation. However, Bell's model does not explicitly take into account experimental parameters such as trap stiffness and elasticity of DNA handles. As a result, we believe that it is subject to more error and is unable to differentiate the small difference in zero force unfolding rates. This notion is supported by the fact that each unfolding rate is significantly decreased in the presence of osmolyte (Fig. 3 *b*), but to a small degree as discussed below.

The apparent unfolding rate at each force in the presence of sorbitol and TMAO decreases 1.39 ± 0.10 and 2.31 ± 0.56 fold, respectively (Table S1), relative to buffer only. Because the apparent rate is related to the activation energy of the process, it is possible to determine the change in activation energy across the overlapped force regimes:

$$k_{app,unf} \propto \exp\left(\frac{-\Delta G^{\ddagger}}{k_B \times T}\right).$$

The average difference in activation energy between these conditions is on the order of thermal noise, which may explain the inability of Bell's model to differentiate zero force-unfolding rates: $\Delta\Delta G^{\ddagger}_{Sorb} = -0.33 \pm 0.07\ k_BT$ and

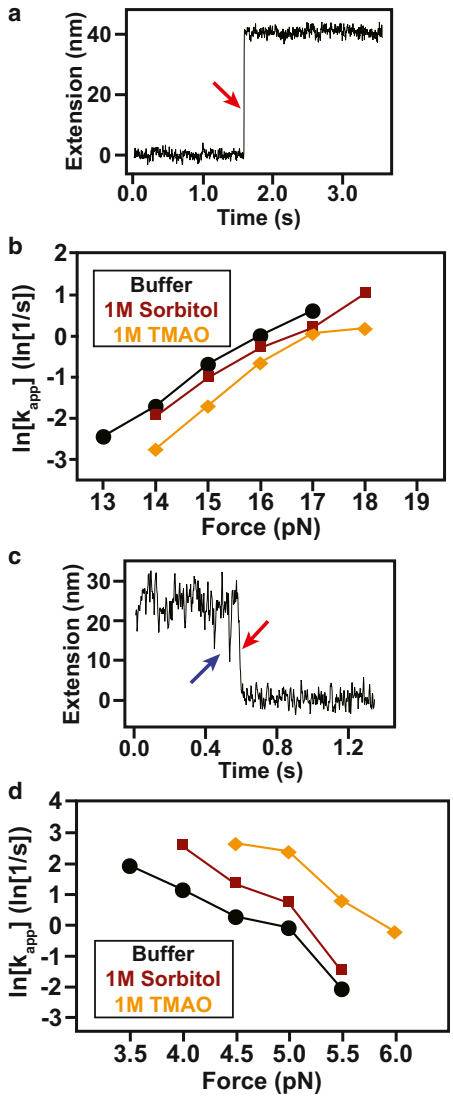

FIGURE 3 Osmolytes affect protein folding kinetics (*a*) Representative force-clamp unfolding transition. Shown is the extension as a function of time with the unfolding transition denoted by the red arrow. Unfolding results in an increase in the relative position of the trap. (*b*) Apparent unfolding kinetics as a function of force. Shown are the apparent kinetic rates under all three conditions tested. Error bars are smaller than the plot points and are thus not visible. (*c*) Representative force-clamp folding transition. Shown is the extension as a function of time with the folding transition denoted by the red arrow. There is a statistically significant on-pathway intermediate observed that is denoted by the blue arrow. (*d*) Apparent folding kinetics as a function of force. Shown are the apparent kinetic rates in all three conditions tested. Due to the significant change in the rates, it was not possible to obtain complete overlap of the force regime. Error bars are smaller than the points on the plot, and are thus not visible. To see this figure in color, go online.

$\Delta\Delta G^{\ddagger}_{TMAO} = -0.82 \pm 0.25\ k_BT$. These changes in activation free energies and folding rates are smaller than what has been reported for other force spectroscopy studies using AFM (22–24). Importantly, our results indicate that at lower concentration of osmolyte and at a lower force regime, osmolytes do not affect unfolding kinetics as much as

previously reported. In short, it is evident that osmolytes marginally decelerate unfolding rates and that all the data are consistent with the mechanical unfolding pathway remaining unperturbed.

Osmolytes accelerate early events in folding

Previous force-spectroscopy experiments in the presence of osmolytes have been unable to directly observe folding because of the high force-regime required for AFM. We empirically noted that the refolding forces observed in the force-ramp experiments (*darker arrows* in Fig. 2 *a*) are slightly higher in the presence of osmolyte, suggesting faster folding rates. Unfortunately, reliable estimates of the refolding force could not be obtained in force-ramp experiments due to the noise in the measurement and hopping behavior at this low force regime. Thus, we carried out force-clamp experiments to directly observe folding and to accurately determine the folding rates of T4* (Fig. 3 *c*). In these measurements, the molecule is populating the unfolded state at time zero and refolds after some time (denoted by the *red arrow*) while being held at a low, constant force. Similarly, we determined the force dependence of the apparent refolding rate constant $k_{\mathrm{app,fold}}$ (Fig. 3 *d*; Table S2).

Two major conclusions can be drawn. First, the apparent folding rate at a given force is accelerated in the presence of osmolyte. The average folding rate is increased in the presence of sorbitol and TMAO by 2.75 ± 1.02 and 13.7 ± 3.8, respectively. These values correspond to $\Delta\Delta G^{\ddagger}_{\mathrm{Sorb}} = 0.96 \pm 0.36\ k_{\mathrm{B}}T$ and $\Delta\Delta G^{\ddagger}_{\mathrm{TMAO}} = 2.59 \pm 0.26\ k_{\mathrm{B}}T$, demonstrating a more pronounced effect than on the unfolding rate deceleration. Second, the folding pathway is not well described by a two-state transition, apparent from the nonlinear dependence of $k_{\mathrm{app,fold}}$ on force. This observation suggests the presence of a folding intermediate. Indeed, despite the increased noise at the lower forces required for folding, the presence of an intermediate state between the unfolded and the native states is clearly apparent (*blue arrow*, Fig. 3 *c*). The weaker force dependence at low forces (owing to the change in the average transition state) indicates that the transition into the intermediate state is more dominant at low forces. Conversely, a higher force dependence is observed when the transition into the native state is more dominant at high forces (4).

From the data it can be inferred that the intermediate observed in the single-molecule folding traces appears to be on-pathway and essentially irreversible once folded to the native state (7). It should be noted that all the constant-force data are consistent with one intermediate state as previously reported in Kaiser et al. (7). Furthermore, upon addition of osmolyte, the kinetics data are still consistent with one intermediate in addition to the binned distribution of distances revealing a single species. It is highly unlikely that multiple intermediates have the same kinetics, extension, and osmolyte sensitivity. This allows the reaction to be schematically represented as:

$$U \underset{k_{I-U}}{\overset{k_{U-I}}{\rightleftharpoons}} I \xrightarrow{k_{I-N}} N,$$

where the unfolded (U) can exchange with the intermediate (I) until it irreversibly folds to the native state (N). To deconvolve the kinetic rate constants, $k_{U\text{-}I}$, $k_{I\text{-}U}$, and $k_{I\text{-}N}$ (where $k_{A\text{-}B}$ represents the rate of going from A to B), we implemented a Bayesian extension of a hidden Markov model (HMM) (40). Advantages of the Bayesian HMM are that it explicitly accounts for experimental noise in addition to distance fluctuations within each state, provides for state assignments as well as a deconvolution of the individual rate constants, and provides more precise values than HMMs by sampling the posterior (Fig. 4 *a*).

At higher forces, $k_{I\text{-}U}$ increases, resulting in lifetimes of the intermediate that are on average too short for our experimental approach to detect. Lower forces, as well as the addition of osmolyte, increase $k_{I\text{-}N}$, similarly reducing the lifetime of the intermediate to the point that it cannot be reliably detected. Nonetheless, we were able to obtain reliable values for all three rate constants at 5.0 pN (Fig. 4 *b*). Due to the nature of the osmophobic effect (i.e., stabilizing folded compact states over more extended states), it may be expected that the rate of formation of either the I state from the U state or the formation of the N state from the I state would be increased significantly as both the U to I and the I to N transitions presumably decrease exposure of the backbone to the solvent. Interestingly, such a conclusion is not borne out of this analysis. The increased apparent folding rate is instead due to a significant increase in $k_{U\text{-}I}$ (i.e., $k_{U\text{-}I,\mathrm{Buffer}} = 2.17\ \mathrm{s}^{-1}$ [1.88 s^{-1}, 2.29 s^{-1}] to $k_{U\text{-}I,1\mathrm{M\ Sorbitol}} = 3.45\ \mathrm{s}_{-1}$ [3.00 s^{-1}, 3.93 s^{-1}] and $k_{U\text{-}I,1\mathrm{M\ TMAO}} = 3.17\ \mathrm{s}^{-1}$

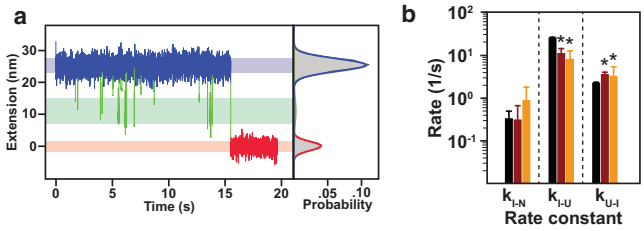

FIGURE 4 Osmolytes specifically affect the first step in folding. (*a*) Representative refolding trace (force-clamp at 5 pN) fit to the Bayesian HMM. The graph shows the extension data with states assigned according to the Bayesian HMM: the unfolded state is shown in blue, the intermediate in green, and the native in red. The width of the shaded bars under the data represents the mean ± 1 SD, which in this case is: $\mu_U \pm \sigma_U = 25.3 \pm 2.0$ nm, $\mu_I \pm \sigma_I = 10.9 \pm 3.8$ nm, and $\mu_N \pm \sigma_N = 0.0 \pm 1.4$ nm. On the right is the probability distribution of the states in this refolding transition. (*b*) Fits of each rate in the folding transition as determined by the BHMM for buffer (*black*), sorbitol (*red*), and TMAO (*orange*). The rates showing significant change are the $k_{I\text{-}U}$ and $k_{U\text{-}I}$ rates denoted by $^{*}p < 0.05$. To see this figure in color, go online.

[2.57 s^{-1}, 5.30 s^{-1}]) and a decrease in $k_{I\text{-}U}$ (i.e., $k_{I\text{-}U,\text{Buffer}} = 24.98\ s^{-1}$ [22.03 s^{-1}, 26.00 s^{-1}] to $k_{I\text{-}U,1\text{M Sorbitol}} = 10.80\ s^{-1}$ [9.51 s^{-1}, 14.08 s^{-1}] and $k_{I\text{-}U,1\text{M TMAO}} = 7.91\ s^{-1}$ [6.25 s^{-1}, 12.50 s^{-1}]) (Fig. 4 *b*).

Interestingly, the rate constant confidence intervals for the final irreversible step have significant overlap, revealing very little, if any, change in the intermediate to native state transition: $k_{I\text{-}N,\ \text{Buffer}} = 0.32\ s^{-1}$ [0.21 s^{-1}, 0.48 s^{-1}], $k_{I\text{-}N,1\text{M Sorbitol}} = 0.30\ s^{-1}$ [0.08 s^{-1}, 0.65 s^{-1}], and $k_{I\text{-}N,1\text{M TMAO}} = 0.86\ s^{-1}$ [0.32 s^{-1}, 1.76 s^{-1}]. Note that the values in brackets represent 95% confidence intervals as previously described in Kaiser et al. (7) and Chodera et al. (40). Although the increase in $k_{U\text{-}I}$ and decrease in $k_{I\text{-}U}$ does not explain the total change in the apparent kinetics (Fig. 3 *d*), these two rates are clearly dominating the changes that are observed in the force-clamp experiments. The modulation of a specific rate constant in the single-molecule folding pathway of T4* has been reported previously. Specifically, the rate of *N* formation from I ($k_{I\text{-}N}$) is decreased when a nascent T4* version folds on the ribosome (7). In direct contrast to the mechanism by which the ribosome affects T4* folding, osmolytes are promoting intermediate formation, an effect that increases the apparent folding rate significantly. Indeed, the population of the intermediate relative to the unfolded state increases significantly from 3.6 to 13.6% and 24.6% from buffer to sorbitol and TMAO, respectively (Fig. 5). Importantly, both classes of osmolytes affect folding by the same mechanism, albeit to different degrees (on a per molar basis).

Structural resolution of the intermediate state using single-molecule COREX: sCOREX

Because single-molecule force spectroscopy experiments conducted in the presence of osmolytes represent a chemomechanical perturbation of the protein, they provide a unique opportunity for characterizing the structural properties of the intermediate state. As noted above, analysis of the constant-force extension traces provides direct access to the contour length change between the I and U states of T4*, corresponding to 96–108 amino acids folded in the intermediate as previously reported in Kaiser et al. (7). Additionally, we do not observe compaction of the intermediate or a deviation from the wormlike chain model as a function of force for the intermediate, supporting the assertion that the intermediate is the same state in the presence of osmolyte. However, we note that the probability of the intermediate changes significantly upon addition of osmolyte, increasing by almost four- and sevenfold in the presence of sorbitol and TMAO, respectively (Fig. 5).

As described previously in Auton and Bolen (12,13) and Auton et al. (14), the equilibrium effect of osmolytes on an intermediate state is based on the amount of ASA relative to the unfolded state. Importantly, because different osmolytes interact with backbone and side-chain surface area to different extents, the relative effect of two or more osmolytes will be unique to each intermediate. If this is the case, it should be possible to use the osmolyte dependence of the intermediate (in one or more osmolytes), in conjunction with the change in contour length from single-molecule experiments, to resolve the structural identity of the intermediate state.

To explore this possibility, we generated potential intermediate state models using a strategy similar to that employed in the COREX algorithm (37), wherein folded regions are treated as adopting the conformation in the native PDB structure and unfolded regions are treated as being extended. Specifically, states were generated by systematically unfolding residues from the N- and C-termini, one residue at a time in all combinations, leaving one contiguously folded region flanked by different amounts of unfolded residues on the N- and C-termini, as described in the Materials and Methods. Because the force-clamp data (Fig. 4) provides the equilibrium between the U and the I states, the energy difference between these states can be determined from the probabilities of each state with and without osmolytes (Fig. 5), thereby providing direct access to the degree to which the I state is stabilized (relative to U) in 1 M TMAO ($\Delta\Delta G = -\text{RT ln } (24.6/3.6) = -1.14$ kcal/mol) and in 1 M sorbitol ($\Delta\Delta G = -\text{RT ln } (13.6/3.6) = -0.79$ kcal/mol).

For comparison, the free energy of all of the potential intermediates can be determined from transfer free-energy values and the difference in solvent ASA between the U and the I state, as described by Auton and Bolen (12,13). According to this relationship, the Gibbs Energy of transfer for any state can be expressed as:

$$\begin{aligned}\Delta\Delta G_{tr,I-U} &= \Delta G\text{tr, I} - \Delta G\text{tr, U} \\ &= -\Big(\sum\nolimits_{i=AA\ type}\Big[n_i\Delta g^{o}_{tr,i,SC}\Delta\alpha^{SC}_{i}\Big] \\ &\quad + \Delta g^{o}_{tr,BB}\sum\nolimits_{i=AA\ type}\big[n_i\Delta\alpha^{BB}_{i}\big]\Big), \qquad (1)\end{aligned}$$

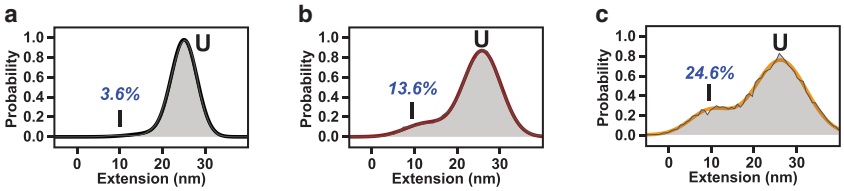

FIGURE 5 Osmolytes stabilize formation of the intermediate (*a–c*) are binned extension distributions for all transitions used for fitting from buffer (*black*), sorbitol (*red*), and TMAO (*orange*), respectively, for unfolded (U) and intermediate (I) states. The mean values of extension have not changed appreciably; however, the relative populations of both have changed significantly from 3.6% to 13.6% and 24.6% from buffer to sorbitol and TMAO, respectively. To see this figure in color, go online.

where $\Delta\Delta G$ is the transfer energy of the intermediate relative to the unfolded state, n_i is the total number of groups of amino acid (AA) type i; Δg_{tr}^{o} is the free energy of transfer for the side-chain (SC), or backbone (BB) to 1 M TMAO or sorbitol; and $\Delta\alpha_i$ is the fractional change in solvent ASA from the unfolded to the intermediate state, which is computed from the expression:

$$\Delta\alpha_i^{bb \text{ or } sc} = \frac{\sum_{j=1}^{n_i}\left(ASA_{i,j,U} - ASA_{i,j,I}\right)}{n_i ASA_{i,\ Gly\cdot X\cdot Gly}}, \qquad (2)$$

where the numerator is summed over all amino acids j of type i, $ASA_{i,j,U}$ is the ASA of the unfolded state, $ASA_{i,j,I}$ is the ASA of the intermediate state, n_i is as defined in Eq. 1, and $ASA_{i,Gly.X.Gly}$ is the standard side-chain or backbone solvent accessibility of Gly-X-Gly tripeptides presenting the maximally exposed surface area (X is the amino acid of type i) (41). See Text S2 in Supporting Materials and Methods for a full derivation.

The ASA of mechanically unfolded T4* is presumably different from the chemically denatured state, complicating structural modeling. Although the fully extended conformation can be readily calculated from physical chemistry principles, T4* is not fully elongated in the refolding experiments. At 5 pN, for example, the unfolded state is ~25 nm more extended than the native state (Fig. 5 *a*) as opposed to the fully elongated state of ~60 nm. A simple linear interpolation between the native state and fully elongated state may provide a first-order estimate of the ~25 nm extended state ASA, but this simplification assumes linearity. To address this concern, we performed SMD to determine ASA and therefore the $\Delta\alpha_i^{bb \text{ or } sc}$ dependence on extension between the native and fully elongated state. Briefly, the system was equilibrated and was subsequently pulled at a constant velocity until fully elongated, similar to Cheng et al. (42), Zheng (43), and Zhang and Lou (44). By performing multiple SMD simulations we were able to determine how $\Delta\alpha_i^{bb \text{ or } sc}$ relates to extension, and to develop statistics on the ASA of the unfolded state (Figs. S1 and S2). From these values, we determined the free energy of transfer for the unfolded state ($\Delta G_{tr,U}$ in Eq. 1) and that of the intermediate ($\Delta G_{tr,I}$ in Eq. 1) as described above. Remarkably, the first-order estimates of ASA from linear interpolation are close to the values calculated from SMD, validating this assumption for future studies.

Using this method, we exhaustively enumerated all possible contiguously folded intermediate states for T4* and determined the free energy of transfer to 1 M sorbitol and TMAO. A plot representing all possible partially folded species with varying unfolded termini are shown in Fig. 6, *a* and *b*, for sorbitol and TMAO, respectively. Several important features emerge. First, there are clear differences in $\Delta\Delta G_{tr,I\text{-}U}$ for unfolding the N-terminus versus the C-terminus in 1 M TMAO and sorbitol relative to the unfolded state (as evidenced by the asymmetry in Fig. 6, *a* and *b*). This asymmetry originates from differences in amino-acid composition between the N- and C-terminal segments of a given length. Second, the magnitude of the free energy difference in 1 M sorbitol is less than in 1 M TMAO, which is expected result given that TMAO is a more potent osmolyte (12,13).

Importantly, when the range of free energies is used to determine intermediates that are consistent with the population changes upon going from buffer to 1 M sorbitol (Fig. 6 *a*) or 1 M TMAO (Fig. 6 *b*), only narrow portions of the potential unfolding combinations for the N- and C-termini agree with experiment (*red-* and *orange-shaded regions*, Fig. 6 *c*). Shown also in Fig. 6 *d* are four potential intermediate states that are tested using this methodology (*I–IV*), which represent unfolding; (*I*) 100 and (*II*) 65 residues from the C-terminus; (*III*) 50 residues each from the N- and C-termini; and (*IV*) 65 residues from the N-terminus.

Inspection of the red and orange regions in Fig. 6 *c* reveals that of all possible states, only a small subset is consistent with both the sorbitol and the TMAO free energy data (see *dark red* in Fig. 6 *c*). Importantly, this minimal overlap is due to the relative differences in how the different osmolytes affect backbone versus side-chain surface area (12,13). In effect, performing the single-molecule experiments in more than one osmolyte significantly constrains the possible states that can produce the observed behavior. When the additional constraint associated with the experimental contour length change (i.e., extension of 96–108 amino acids) is also applied (Fig. 6 *c*, *yellow diagonal bar*), only one region is found where there is an overlap between all three of the experimental constraints (*cyan-shaded region*, Fig. 6 *c*).

The results indicate that the structural character of the intermediate state is most consistent with the C-terminal domain of T4* being folded and the N-terminal domain being unfolded (Fig. 6 *d*, *IV*). Remarkably, the predicted intermediate is consistent with two previous experimental observations. First, the division of the structure falls precisely at the known structural domain boundary of T4* previously identified by x-ray crystallography (45). Second, the N-terminus being unfolded is consistent with the known relative stability of this domain obtained from both ensemble experimental (46) and theoretical (47) studies. In short, these results suggest that the constraints imposed by performing optical tweezers experiments in multiple osmolytes provides sufficient information, when combined with the experimental contour length change, to distinguish the structural character of nativelike folding intermediates.

We note that recent studies have questioned whether general transfer free energy models based on surface area can mechanistically capture the relative energetic contribution of osmolytes to the transfer free energy of side chains versus backbone (48,49). We make no claims about the

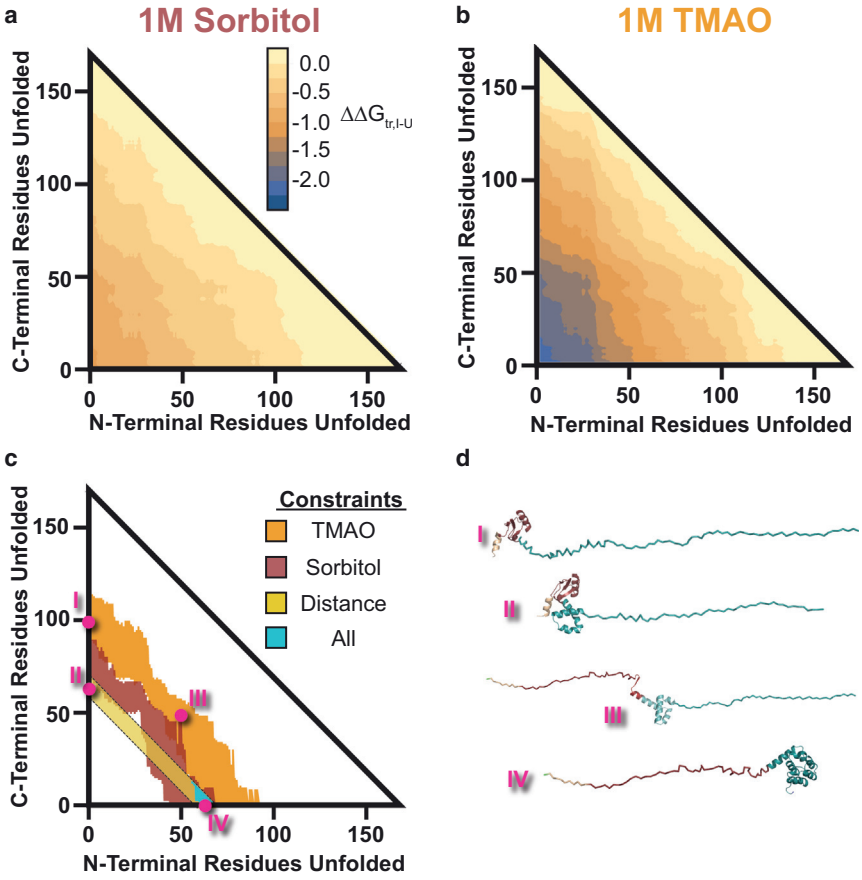

FIGURE 6 Experimental discrimination of structural models of the T4* folding intermediate. (*a*) Plot of the transfer free-energy difference between the I and U state ($\Delta\Delta G_{tr,I\text{-}U}$) for every possible contiguously folded intermediate of T4* to 1 M sorbitol. The axes represent the portion of the N-terminal or C-terminal residues unfolded in the intermediate. The values are shaded according to value as denoted by the key. (*b*) Shown is the same plot as (*a*), except for 1 M TMAO. Of note is that the values have higher magnitude, as expected from transfer free-energy models. (*c*) Shown are the experimental constraints on potential intermediates that are considered. Shaded in orange and red are intermediates that are consistent with the population changes in going from buffer to 1 M TMAO and 1 M sorbitol, respectively. The yellow diagonal bar is the dimensional contour-length-based constraint from the BHMM. Shaded in cyan are the intermediates consistent with all three constraints. These are all intermediates where the N-terminal domain is mostly unfolded and the C-terminal domain is primarily folded. (*d*) Potential structural models of intermediates. Color-coding is identical to Fig. 1 *a*. (*I*) Depicted is the N-terminal subdomain that is consistent with the population constraint of TMAO (folded amino acids 60–72). (*II*) Depicted is the N-terminal subdomain portion along with C-terminal subdomain portion folded to be consistent with distance restraint (folded amino acids 96–108). (*III*) Depicted is an intermediate that has 50 amino acids of the N- and C-terminus unfolded. This intermediate is consistent with both population restraints. (*IV*) Depicted is the C-terminal subdomain structural model that is consistent with both constraints (C-terminus). This is the only intermediate that is consistent with all three pieces of experimental data. To see this figure in color, go online.

underlying mechanism, and in fact, whether or not the molecular origins of the osmolyte effect are understood, the parameterization of the transfer free energies in terms of surface area is no less predictive, as clearly demonstrated by Auton and Bolen (12,13). As such, this analysis provides quantitative insight into the structural character of the intermediate.

Finally, it is interesting to speculate on the potential implications of such an approach to systems in which structure is not known or in the case of intrinsically disordered proteins (IDPs). It is clear that marginally stable proteins and certain IDPs fold cooperatively upon the addition of ligands and osmolytes to their functional state(s) (50–52). Performing the experiments described here, under different osmolyte concentrations and forces, can yield multidimensional information about the states that are accessed during folding/unfolding. Because the transfer free energies have been shown here to be valid in single-molecule force spectroscopy experiments, it should be possible to study IDPs under osmolyte and force conditions where the folding is more probable, and to extrapolate the probabilities to functional conditions (i.e., 0 pN force and 0 M osmolytes), thereby providing a lens into the functional conformational transitions of IDPs. The applicability of this strategy to the analysis of IDPs awaits further study.

CONCLUSIONS

To our knowledge, we believe this study represents the first use of the osmophobic effect at the single-molecule level to discriminate between structural models of the intermediate state populated during folding. We observe an increase in folding rate consistent with what has previously been reported for the effect of osmolyte. However, our ability to directly observe folding together with a robust method to determine individual rate constants from the single-molecule traces (Fig. 4 *b*) reveals surprising details of how osmolytes modulate T4* folding. Strikingly, formation of a folding intermediate is specifically modulated in the first step of the folding pathway: i.e., the population of the intermediate changes because $k_{U\text{-}I}$ and $k_{I\text{-}U}$ change, while $k_{I\text{-}N}$ is relatively unperturbed. This finding is unexpected because approximately one-third of the molecule remains unfolded in the intermediate state, leaving a significant

portion of the peptide backbone exposed to solvent. How is it possible, then, that $k_{I\text{-}N}$ is not affected by osmolytes? Because the rate depends on how osmolyte is affecting the energy of the intermediate state relative to the transition state, the lack of a difference in $k_{I\text{-}N}$, with and without osmolyte suggests that the surface area exposed in the transition state, relative to the intermediate state, is approximately the same.

Regardless of the origin of the effect, the functional implications are clear. Low concentrations of osmolytes decrease the rate of the transition from I to U, in effect minimizing the probability of an excursion to higher energy states. This suggests an osmolyte-driven dampening of dynamics of the protein, an assertion that is consistent with results obtained from hydrogen exchange studies (53). We note that our results report the effect of osmolyte on one protein (T4*). The fact that we obtain similar results using two different osmolytes applied to one protein of course does not mean that the results will be the same for all proteins. Nonetheless, the results presented here reveal that single-molecule force spectroscopy provides a powerful tool to understand the impact of osmolytes on protein stability.

We note that at least in the case of T4*, osmolytes primarily affect the rate of the U to I transition, while the ribosome was recently shown to affect the I to N transition (7), indicating that osmolytes and ribosomes exert their impact on different parts of the T4* folding reaction. Whether this effect is a general phenomenon remains to be seen. However, it is interesting to speculate on the benefits of biological systems being able to evolve orthogonal mechanisms that presumably can be effective both together and separately. Did osmolytes evolve so as to minimize the potential of adversely affecting cotranslational folding in organisms where osmolytes are colocalized with functioning ribosomes?

Perhaps most importantly, our results demonstrate that using osmolytes as a chemo-mechanical perturbation is a powerful approach for gleaning structural information about intermediates in the form of a second metric (i.e., solvent-accessible surface area). Although applied here to data obtained from optical tweezers, the strategy, in principle, is not limited to force spectroscopy. Other techniques, such as single-molecule fluorescence spectroscopy, providing access to changes in populations of states in different osmolyte concentrations, can also provide information about surface area. Whether this is indeed the case awaits further studies, although the relationship between Förster resonance energy transfer efficiency and absolute distance changes may be less certain than with optical tweezers.

SUPPORTING MATERIAL

Supporting Materials and Methods, two figures, and two tables are available at http://www.biophysj.org/biophysj/supplemental/S0006-3495(16)00137-5.

AUTHOR CONTRIBUTIONS

H.N.M., D.T., C.M.K., and V.J.H. designed the research; H.N.M. performed the research; and H.N.M., D.T., C.M.K., and V.J.H analyzed the data and wrote the article.

ACKNOWLEDGMENTS

We thank Steve Smith for his advice in building the optical tweezers instrument, and James Rives for assistance with DNA handle generation. We also thank all members of the Hilser and Kaiser labs for thoughtful discussions.

This work was supported by the National Institutes of Health grants No. R01-GM63747 to V.J.H. and T32-GM008403 to the Program in Molecular Biophysics (Johns Hopkins University).

SUPPORTING CITATIONS

Reference (54) appears in the Supporting Material.

REFERENCES

1. Cecconi, C., E. A. Shank, …, S. Marqusee. 2005. Direct observation of the three-state folding of a single protein molecule. *Science.* 309:2057–2060.
2. Guinn, E. J., B. Jagannathan, and S. Marqusee. 2015. Single-molecule chemo-mechanical unfolding reveals multiple transition state barriers in a small single-domain protein. *Nat. Commun.* 6:6861.
3. Jagannathan, B., and S. Marqusee. 2013. Protein folding and unfolding under force. *Biopolymers.* 99:860–869.
4. Jagannathan, B., P. J. Elms, …, S. Marqusee. 2012. Direct observation of a force-induced switch in the anisotropic mechanical unfolding pathway of a protein. *Proc. Natl. Acad. Sci. USA.* 109:17820–17825.
5. Shank, E. A., C. Cecconi, …, C. Bustamante. 2010. The folding cooperativity of a protein is controlled by its chain topology. *Nature.* 465:637–640.
6. Gao, Y., S. Zorman, …, Y. Zhang. 2012. Single reconstituted neuronal SNARE complexes zipper in three distinct stages. *Science.* 337:1340–1343.
7. Kaiser, C. M., D. H. Goldman, …, C. Bustamante. 2011. The ribosome modulates nascent protein folding. *Science.* 334:1723–1727.
8. Maillard, R. A., G. Chistol, …, C. Bustamante. 2011. ClpX(P) generates mechanical force to unfold and translocate its protein substrates. *Cell.* 145:459–469.
9. Gebhardt, J. C., T. Bornschlögl, and M. Rief. 2010. Full distance-resolved folding energy landscape of one single protein molecule. *Proc. Natl. Acad. Sci. USA.* 107:2013–2018.
10. Liphardt, J., B. Onoa, …, C. Bustamante. 2001. Reversible unfolding of single RNA molecules by mechanical force. *Science.* 292:733–737.
11. Stigler, J., F. Ziegler, …, M. Rief. 2011. The complex folding network of single calmodulin molecules. *Science.* 334:512–516.
12. Auton, M., and D. W. Bolen. 2005. Predicting the energetics of osmolyte-induced protein folding/unfolding. *Proc. Natl. Acad. Sci. USA.* 102:15065–15068.
13. Auton, M., and D. W. Bolen. 2007. Application of the transfer model to understand how naturally occurring osmolytes affect protein stability. *Methods Enzymol.* 428:397–418.
14. Auton, M., J. Rösgen, …, D. W. Bolen. 2011. Osmolyte effects on protein stability and solubility: a balancing act between backbone and side-chains. *Biophys. Chem.* 159:90–99.
15. Street, T. O., D. W. Bolen, and G. D. Rose. 2006. A molecular mechanism for osmolyte-induced protein stability. *Proc. Natl. Acad. Sci. USA.* 103:13997–14002.

16. Yancey, P. H., M. E. Clark, …, G. N. Somero. 1982. Living with water stress: evolution of osmolyte systems. *Science.* 217:1214–1222.

17. Russo, A. T., J. Rösgen, and D. W. Bolen. 2003. Osmolyte effects on kinetics of FKBP12 C22A folding coupled with prolyl isomerization. *J. Mol. Biol.* 330:851–866.

18. Pradeep, L., and J. B. Udgaonkar. 2004. Osmolytes induce structure in an early intermediate on the folding pathway of barstar. *J. Biol. Chem.* 279:40303–40313.

19. Mukaiyama, A., Y. Koga, …, S. Kanaya. 2008. Osmolyte effect on the stability and folding of a hyperthermophilic protein. *Proteins.* 71: 110–118.

20. Lin, S. L., A. Zarrine-Afsar, and A. R. Davidson. 2009. The osmolyte trimethylamine-N-oxide stabilizes the Fyn SH3 domain without altering the structure of its folding transition state. *Protein Sci.* 18: 526–536.

21. Garcia-Manyes, S., L. Dougan, and J. M. Fernández. 2009. Osmolyte-induced separation of the mechanical folding phases of ubiquitin. *Proc. Natl. Acad. Sci. USA.* 106:10540–10545.

22. Aioanei, D., S. Lv, …, M. Brucale. 2011. Single-molecule-level evidence for the osmophobic effect. *Angew. Chem. Int. Ed. Engl.* 50:4394–4397.

23. Aioanei, D., I. Tessari, …, M. Brucale. 2011. Observing the osmophobic effect in action at the single molecule level. *Proteins.* 79:2214–2223.

24. Aioanei, D., M. Brucale, …, B. Samorì. 2012. Worm-like Ising model for protein mechanical unfolding under the effect of osmolytes. *Biophys. J.* 102:342–350.

25. Matsumura, M., and B. W. Matthews. 1989. Control of enzyme activity by an engineered disulfide bond. *Science.* 243:792–794.

26. Parker, M. J., and S. Marqusee. 1999. The cooperativity of burst phase reactions explored. *J. Mol. Biol.* 293:1195–1210.

27. Cellitti, J., R. Bernstein, and S. Marqusee. 2007. Exploring subdomain cooperativity in T4 lysozyme II: uncovering the C-terminal subdomain as a hidden intermediate in the kinetic folding pathway. *Protein Sci.* 16:852–862.

28. Beckett, D., E. Kovaleva, and P. J. Schatz. 1999. A minimal peptide substrate in biotin holoenzyme synthetase-catalyzed biotinylation. *Protein Sci.* 8:921–929.

29. Yin, J., A. J. Lin, …, C. T. Walsh. 2006. Site-specific protein labeling by Sfp phosphopantetheinyl transferase. *Nat. Protoc.* 1:280–285.

30. Yin, J., P. D. Straight, …, C. T. Walsh. 2005. Genetically encoded short peptide tag for versatile protein labeling by Sfp phosphopantetheinyl transferase. *Proc. Natl. Acad. Sci. USA.* 102:15815–15820.

31. Fuller, D. N., G. J. Gemmen, …, D. E. Smith. 2006. A general method for manipulating DNA sequences from any organism with optical tweezers. *Nucleic Acids Res.* 34:e15.

32. Smith, S. B., Y. Cui, and C. Bustamante. 1996. Overstretching B-DNA: the elastic response of individual double-stranded and single-stranded DNA molecules. *Science.* 271:795–799.

33. Smith, S. B., Y. Cui, and C. Bustamante. 2003. Optical-trap force transducer that operates by direct measurement of light momentum. *Methods Enzymol.* 361:134–162.

34. Smith, S. B., L. Finzi, and C. Bustamante. 1992. Direct mechanical measurements of the elasticity of single DNA molecules by using magnetic beads. *Science.* 258:1122–1126.

35. Phillips, J. C., R. Braun, …, K. Schulten. 2005. Scalable molecular dynamics with NAMD. *J. Comput. Chem.* 26:1781–1802.

36. Best, R. B., X. Zhu, …, A. D. MacKerell, Jr. 2012. Optimization of the additive CHARMM all-atom protein force field targeting improved sampling of the backbone φ, ψ and side-chain χ^1 and χ^2 dihedral angles. *J. Chem. Theory Comput.* 8:3257–3273.

37. Hilser, V. J., and E. Freire. 1996. Structure-based calculation of the equilibrium folding pathway of proteins. Correlation with hydrogen exchange protection factors. *J. Mol. Biol.* 262:756–772.

38. Dudko, O. K., G. Hummer, and A. Szabo. 2008. Theory, analysis, and interpretation of single-molecule force spectroscopy experiments. *Proc. Natl. Acad. Sci. USA.* 105:15755–15760.

39. Bell, G. I. 1978. Models for the specific adhesion of cells to cells. *Science.* 200:618–627.

40. Chodera, J. D., P. J. Elms, …, N. S. Hinrichs. 2011. Bayesian hidden Markov model analysis of single-molecule force spectroscopy: characterizing kinetics under measurement uncertainty. arXiv 1108.1430.

41. Lee, B., and F. M. Richards. 1971. The interpretation of protein structures: estimation of static accessibility. *J. Mol. Biol.* 55:379–400.

42. Cheng, C. L., M. Z. Zhang, and G. J. Zhao. 2014. Mechanical stability and thermal conductivity of β-barrel in green fluorescent protein by steered molecular dynamics. *Res. Adv.* 4:6513–6516.

43. Zheng, W. 2014. All-atom and coarse-grained simulations of the forced unfolding pathways of the SNARE complex. *Proteins.* 82:1376–1386.

44. Zhang, Y., and J. Lou. 2012. The Ca^{2+} influence on calmodulin unfolding pathway: a steered molecular dynamics simulation study. *PLoS One.* 7:e49013.

45. Matthews, B. W., and S. J. Remington. 1974. The three dimensional structure of the lysozyme from bacteriophage T4. *Proc. Natl. Acad. Sci. USA.* 71:4178–4182.

46. Llinás, M., B. Gillespie, …, S. Marqusee. 1999. The energetics of T4 lysozyme reveal a hierarchy of conformations. *Nat. Struct. Biol.* 6:1072–1078.

47. Hilser, V. J., B. D. Townsend, and E. Freire. 1997. Structure-based statistical thermodynamic analysis of T4 lysozyme mutants: structural mapping of cooperative interactions. *Biophys. Chem.* 64:69–79.

48. Canchi, D. R., and A. E. García. 2011. Backbone and side-chain contributions in protein denaturation by urea. *Biophys. J.* 100:1526–1533.

49. Moeser, B., and D. Horinek. 2014. Unified description of urea denaturation: backbone and side chains contribute equally in the transfer model. *J. Phys. Chem. B.* 118:107–114.

50. Baskakov, I., and D. W. Bolen. 1998. Forcing thermodynamically unfolded proteins to fold. *J. Biol. Chem.* 273:4831–4834.

51. Mello, C. C., and D. Barrick. 2003. Measuring the stability of partly folded proteins using TMAO. *Protein Sci.* 12:1522–1529.

52. Li, J., H. N. Motlagh, …, V. J. Hilser. 2012. Thermodynamic dissection of the intrinsically disordered N-terminal domain of human glucocorticoid receptor. *J. Biol. Chem.* 287:26777–26787.

53. Qu, Y., and D. W. Bolen. 2003. Hydrogen exchange kinetics of RNase A and the urea:TMAO paradigm. *Biochemistry.* 42:5837–5849.

54. Ando, N., B. Barstow, …, S. M. Gruner. 2008. Structural and thermodynamic characterization of T4 lysozyme mutants and the contribution of internal cavities to pressure denaturation. *Biochemistry.* 47:11097–11109.

55. Bustamante, C., J. F. Marko, …, S. Smith. 1994. Entropic elasticity of lambda-phage DNA. *Science.* 265:1599–1600.

Biophysical Journal, Volume *110*

Supplemental Information

Single-Molecule Chemo-Mechanical Spectroscopy Provides Structural Identity of Folding Intermediates

Hesam N. Motlagh, Dmitri Toptygin, Christian M. Kaiser, and Vincent J. Hilser

Supplementary Text for

Single-molecule chemo-mechanical spectroscopy provides structural resolution of protein folding intermediates

Hesam N. Motlagh*[a], Dmitri Toptigyn[b], Christian M. Kaiser[b], and Vincent J. Hilser*[a,b]

[a]T.C. Jenkins Department of Biophysics, [b]Department of Biology,

The Johns Hopkins University, Baltimore, Maryland 21218

*Correspondence: VJH (Hilser@jhu.edu) or HNM (Hnekoor1@jhu.edu)

Tel: 410-516-6072; Fax: 410-516-5213

Supplementary Text S1 – Unfolding rates are marginally decelerated in the presence of osmolytes

The mean unfolding forces ($<F_{unf}>$) obtained in the presence and absence of osmolytes overlap significantly: $F_{unf,buffer}$ = 17.6±1.9pN (N=224), $F_{unf,1M\ Sorbitol}$ = 18.2±2.1pN (N=288), and $F_{unf,1M\ TMAO}$ = 18.2±2.2pN (N=340) which initially suggests no significant change in the unfolding rates. To quantitatively evaluate the unfolding, several force-ramp data sets were collected and analyzed using a model that converts the force rupture distribution to an intrinsic lifetime and distance to transition state (1). The model reveals that the distance to the transition state does not change appreciably in the presence of either osmolyte: $\Delta x^{\ddagger}_{Buffer}$ = 2.7±0.1nm, $\Delta x^{\ddagger}_{1M\ Sorbitol}$ = 2.8±0.1nm, and $\Delta x^{\ddagger}_{1M\ TMAO}$ = 2.3±0.1nm. Although the value for TMAO differs somewhat from the sorbitol and buffer values, this difference is likely an artifact of the model being sensitive to the shape of the distribution. Indeed, constant-force experiments in the main text reveal that $\Delta x^{\ddagger}$ is not significantly different under the three different conditions, consistent with previously reported findings (2). Taken together, these results suggest that neither TMAO nor sorbitol change the unfolding pathway of T4*.

We note that the distance to the transitions state determined in our experiments, applying force to the termini of T4*, is unusually large. Most globular proteins exhibit distances to the transition state of less than 1 nm, reflecting the brittle nature of stably folded proteins (3). Native T4* has a radius of gyration (R_g) of ~2nm (4). The $\Delta x^{\ddagger}$ values determined here and previously (5) suggest that the molecule can be extended by approximately this length before crossing the barrier to unfolding. We believe that the origin of the large $\Delta x^{\ddagger}$ values is likely the unstable N-terminal A-helix region (6) that may deform easily under mechanical load before the barrier to unfolding is crossed (Fig. 1A). Regardless of the origin of the large absolute values, $\Delta x^{\ddagger}$ appears to be the same in all cases, indicating that osmolytes do not appreciably affect the position of the barrier to unfolding.

The unfolding force distributions, analyzed as described above (1), suggest a change in the folded state lifetimes extrapolated to zero force (τ_o) when $\Delta x^{\ddagger}$ is fixed at 2.7nm. $\tau_{o,Buffer}$ = 46,101±188s, $\tau_{o,1M\ Sorbitol}$ = 69,916±261s, and $\tau_{o,1M\ TMAO}$ = 71,698±562s. Determining τ_o required extrapolation over a relatively large force range and the exclusion of transition state sliding, imparting some uncertainty onto the determined values. Nevertheless, given that osmolytes stabilize the native states of proteins, our results are not unexpected, as osmolytes have been shown to decrease unfolding rates both in bulk (7-9) and at the single-molecule level (2, 10-12). Taken together, the data are consistent with a slight decrease in the unfolding rate and no significant change in the pathway. These conclusions are supported by the constant force experiments conducted in the main text.

Supplementary Text S2 – Derivation of transfer free energy for intermediate states

The single-molecule folding traces yield direct access to the probability of the intermediate (P_I) relative to the unfolded state. All calculations below only consider the change in probability from Buffer to 1M TMAO. Since we have measured $P_{I,Buffer}$ and $P_{I,1M\ TMAO}$, we can calculate the free energy change of the chemo-mechanical perturbation using a Boltzmann distribution as follows:

$$\frac{P_{I,1M\,TMAO}}{P_{I,Buffer}} = \frac{\exp\left(\frac{\Delta G_{I,1M\,TMAO}}{R*T}\right)}{\exp\left(\frac{\Delta G_{I,Buffer}}{R*T}\right)} = \exp\left(\frac{-\left[\Delta G_{I,1M\,TMAO} - \Delta G_{I,Buffer}\right]}{R*T}\right) \qquad \text{(Eq. S1)}$$

where $\Delta G_{I,1M\ TMAO}$ and $\Delta G_{I,Buffer}$ are the free energies of the intermediate state relative to the unfolded state (i.e. reference state), R is the universal gas constant, and T is the absolute

temperature. Implicit in this formalism is the assumption of equilibrium. We consider this a justified assumption given the low force regime (i.e. near equilibrium) and the subsequent predictive capabilities of the model generate. Should the assumption of equilibrium be incorrect, the predictive capabilities would be compromised.

The value in the numerator on the right side of Eq. S1 can be re-written as a function of the transfer free energy of the intermediate and unfolded states:

$$\Delta G_{I,1M\ TMAO} - \Delta G_{I,Buffer} = G_{I,1M\ TMAO} - G_{U,1M\ TMAO} - G_{I,Buffer} + G_{U,Buffer} = \Delta G_{I,tr} - \Delta G_{U,tr} \quad \text{(Eq. S2)}$$

Where $\Delta G_{I,tr}$ and $\Delta G_{U,tr}$ are the transfer free energies of the intermediate and unfolded state to 1M TMAO respectively. Both of these transfer free energies depend on the accessible surface area (ASA) of the states in question. As mentioned in the main text, we treat the intermediate state as a contiguously folded portion of the protein that has the same ASA as the crystallographic structure. This is justified since the intermediate is on-pathway and is presumably native-like.

Let us consider a general intermediate within the context of the derivation above: the intermediate has a contiguously folded portion of amino acids N_{tr} through C_{tr}, where these values are integers corresponding to the amino acid numbers that are the boundaries for the folded portion of the molecule (Note: $1 \leq N_{tr} < C_{tr} \leq 164$). Several immediate relationships become apparent from this formalism. For instance, the unfolded portion of the molecule is amino acids 1 through N_{tr-1} and C_{tr+1} through 164 (the number of amino acids in T4*). Since these residues are also unfolded in the unfolded state their transfer free energies in Eq. S2 cancels out. The transfer free energy in Eq. S2 actually corresponds to the transfer free energy of the folded portion (i.e. amino acids N_{tr} through C_{tr}). This can be appreciated by calculating the free energy of both states:

$$\Delta G_{I,tr} = \sum_{i=1}^{N_{tr}-1}(\Delta\alpha_i^{SC}\Delta g_{tr,i,SC}^{o} + \Delta\alpha_i^{BB}\Delta g_{tr,i,BB}^{o}) + \sum_{j=C_{tr}+1}^{164}(\Delta\alpha_j^{SC}\Delta g_{tr,j,SC}^{o} + \Delta\alpha_j^{BB}\Delta g_{tr,j,BB}^{o}) \quad \text{(Eq. S3)}$$

and

$$\Delta G_{U,tr} = \sum_{i=1}^{164}(\Delta\alpha_i^{SC}\Delta g_{tr,i,SC}^{o} + \Delta\alpha_i^{BB}\Delta g_{tr,i,BB}^{o}) \quad \text{(Eq. S4)}$$

where i is the amino acid type from the primary sequence, Δg^{o}_{tr} is the free energy of transfer for the side-chain (SC) or backbone (BB) to 1M TMAO, and $\Delta\alpha_i$ is the fractional change in solvent ASA from the unfolded to the intermediate state (13, 14).

The $\Delta\alpha_i$ values in Eqs. S3 and S4 require estimates of the ASA of the unfolded and intermediate states:

$$\Delta\alpha_i^{bb\ or\ sc} = \frac{\sum_{j=1}^{n_i}(ASA_{i,j,U} - ASA_{i,j,I})}{n_i ASA_{i,Gly\cdot X\cdot Gly}} \quad \text{(Eq. S5)}$$

Where the numerator is summed over all amino acids j of type i, $ASA_{i,jU}$ is the ASA of the unfolded state, $ASA_{i,j,I}$ is the ASA of the intermediate state, n_i is the total number of groups of amino acid (AA) type i, and $ASA_{i,Gly.X.Gly}$ is the standard side-chain or backbone solvent accessibility of Gly-X-Gly tripeptides presenting the maximally exposed surface area (X it the amino acid of type i) (15). The values for α are calculated based on the steered molecular dynamics simulations to represent the unfolded state (see SI text 3 below).

Substituting Eqs. S3 and S4 into Eq. S2 results in a canceling out of terms such that now Eq. S2 reduces to:

$$\Delta G_{I,1M\ TMAO} - \Delta G_{I,Buffer} = -\sum_{N_{tr}}^{C_{tr}}(\Delta\alpha_i^{SC}\Delta g_{tr,i,SC}^{o} + \Delta\alpha_i^{BB}\Delta g_{tr,i,BB}^{o}) \quad \text{(Eq. S6)}$$

where all the terms are defined identically to Eqs. S3 and S4. The right hand side of Eq. S6 is actually a calculation of the transfer free energy of the folded portion of the intermediate to 1M TMAO. In particular, Eq. S6 is what was used to calculate the heat map in Figure 6B and to relate the experimental probability changes to the contour plot (i.e. by substituting Eq. S6 into Eq. S1). In all subsequent calculations, each amino acid was treated as either folded or not based on the intermediate boundaries defined by N_{tr} and C_{tr}. This approach was used for 1M Sorbitol as well which generated figure 6A.

References:

1. Dudko OK, Hummer G, & Szabo A (2008) Theory, analysis, and interpretation of single-molecule force spectroscopy experiments. *Proc Natl Acad Sci U S A* 105(41):15755-15760.
2. Aioanei D, Brucale M, Tessari I, Bubacco L, & Samori B (2012) Worm-like Ising model for protein mechanical unfolding under the effect of osmolytes. *Biophysical journal* 102(2):342-350.
3. Jagannathan B, Elms PJ, Bustamante C, & Marqusee S (2012) Direct observation of a force-induced switch in the anisotropic mechanical unfolding pathway of a protein. *Proc Natl Acad Sci U S A* 109(44):17820-17825.
4. Ando N*, et al.* (2008) Structural and thermodynamic characterization of T4 lysozyme mutants and the contribution of internal cavities to pressure denaturation. *Biochemistry* 47(42):11097-11109.
5. Kaiser CM, Goldman DH, Chodera JD, Tinoco I, & Bustamante C (2011) The Ribosome Modulates Nascent Protein Folding. *Science* 334(6063):1723-1727.
6. Hilser VJ, Townsend BD, & Freire E (1997) Structure-based statistical thermodynamic analysis of T4 lysozyme mutants: Structural mapping of cooperative interactions. *Biophys Chem* 64(1-3):69-79.
7. Russo AT, Rosgen J, & Bolen DW (2003) Osmolyte effects on kinetics of FKBP12 C22A folding coupled with prolyl isomerization. *Journal of molecular biology* 330(4):851-866.
8. Mukaiyama A, Koga Y, Takano K, & Kanaya S (2008) Osmolyte effect on the stability and folding of a hyperthermophilic protein. *Proteins* 71(1):110-118.
9. Pradeep L & Udgaonkar JB (2004) Osmolytes induce structure in an early intermediate on the folding pathway of barstar. *The Journal of biological chemistry* 279(39):40303-40313.
10. Aioanei D*, et al.* (2011) Single-molecule-level evidence for the osmophobic effect. *Angewandte Chemie* 50(19):4394-4397.
11. Aioanei D, Tessari I, Bubacco L, Samori B, & Brucale M (2011) Observing the osmophobic effect in action at the single molecule level. *Proteins* 79(7):2214-2223.
12. Garcia-Manyes S, Dougan L, & Fernandez JM (2009) Osmolyte-induced separation of the mechanical folding phases of ubiquitin. *Proc Natl Acad Sci U S A* 106(26):10540-10545.
13. Auton M & Bolen DW (2007) Application of the Transfer Model to Understanding How Naturally Occuring Osmolytes Affect Protein Stability. *Methods in Enzymology* 428:397-418.
14. Auton M & Bolen DW (2005) Predicting the energetics of osmolyte-induced protein folding/unfolding. *Proceedings of the National Academy of Sciences of the United States of America* 102(42):15065-15068.
15. Lee B & Richards FM (1971) The interpretation of protein structures: estimation of static accessibility. *Journal of molecular biology* 55(3):379-400.

Supplementary Table S1 – Constant-force unfolding rate constants and statistics

Table 1 – Unfolding Kinetics

Condition	HKM		Sorbitol				TMAO			
Force (pN)	k_{app} [a]	N [b]	k_{app} [a]	N [b]	Change [c]	ΔΔG(kb*T) [d]	k_{app} [a]	N [b]	Change [c]	ΔΔG(kb*T) [d]
13	0.0854 ± 0.0008	67	N/A				N/A			
14	0.1781 ± 0.0025	100	0.1383 ± 0.0035	59	1.29	-0.25	0.0628 ± 0.0006	124	2.84	-1.04
15	0.4945 ± 0.0041	140	0.3527 ± 0.0067	73	1.40	-0.34	0.1796 ± 0.0010	186	2.75	-1.01
16	0.9898 ± 0.0068	138	0.7290 ± 0.0071	81	1.36	-0.31	0.5123 ± 0.0033	132	1.93	-0.66
17	1.8131 ± 0.0125	157	1.1872 ± 0.0132	79	1.53	-0.42	1.0446 ± 0.0150	131	1.74	-0.55
18	N/A		2.7291 ± 0.0965	21		N/A	1.1807 ± 0.0192	74		N/A
			Average		1.39	-0.33	Average		2.31	-0.82
			StdDev		0.10	0.07	StdDev		0.56	0.25

Supplementary Table S2 – Constant-force folding rate constants and statistics

Condition	HKM		Sorbitol				TMAO			
Force (pN)	k_{app} [a]	N	k_{app} [a]	N [b]	Change [c]	ΔΔG(kb*T) [d]	k_{app} [a]	N [b]	Change [c]	ΔΔG(kb*T) [d]
3.5	6.6049 ± 0.1382	29	N/A				N/A			
4	3.0043 ± 0.0316	92	12.3369 ± 0.3832	59	4.11	1.41	N/A			
4.5	1.2467 ± 0.0263	154	3.5842 ± 0.0848	55	2.87	1.06	13.6907 ± 0.1844	106	10.98	2.40
5	0.8686 ± 0.0060	236	1.9445 ± 0.0533	112	2.24	0.81	10.4996 ± 0.1715	264	12.09	2.49
5.5	0.1177 ± 0.0062	60	0.2073 ± 0.0118	66	1.76	0.57	2.1226 ± 0.0468	84	18.04	2.89
6	N/A		N/A				0.7654 ± 0.0091	136		N/A
			Average		2.75	0.96	Average		13.70	2.59
			StdDev		1.02	0.36	StdDev		3.80	0.26

[a]The reported values for k_{app} are the apparent rates that describe the single-exponential lifetime distributions at each force for unfolding (Table 1) and folding (Table 2).
[b]N is the number of transitions observed at that force across all molecules. The approximate number of transitions from each molecule was approximately the same and thus the statistics are robustly determined.
[c]The reported change in the rate constant is calculated relative to HKM (Buffer) conditions.
[d]The change in activation free energy is calculated based on the relative change of the apparent rate constants.

Supplementary Figure S1 – Alpha values from steered molecular dynamics simulations

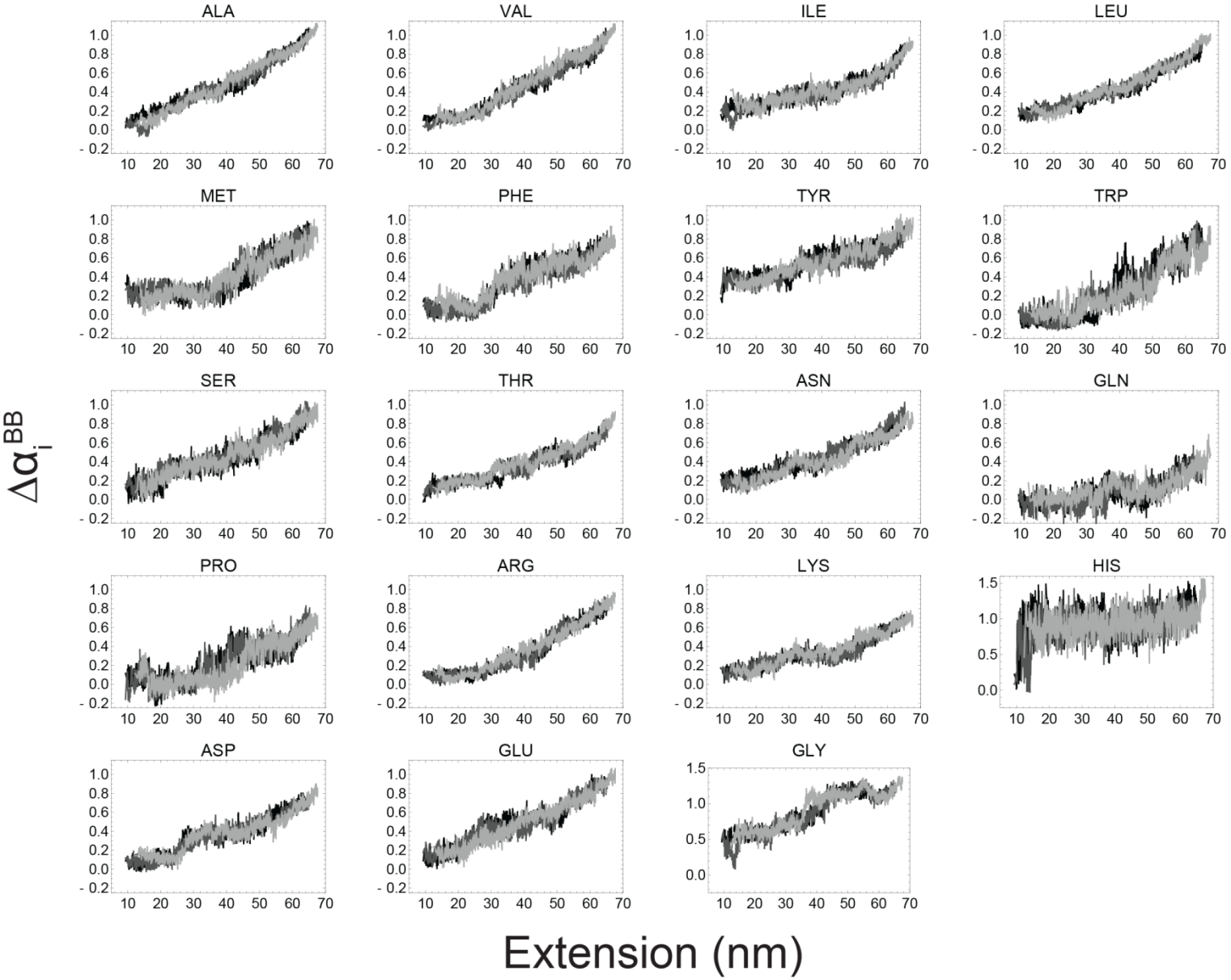

Supplementary Figure S1 – Shown are the calculated Δα values for all amino acids in T4* from the steered molecular dynamics simulations. These values are for the backbone (BB) and all three simulations are overlaid showing excellent reproducibility. Note that the majority of amino acids are simply a line between the initial Δα from the crystal structure to 1.0 when fully extended. Average values corresponding to the dimensions of the unfolded state from the BHMM were used in transfer free energy calculations of the intermediate (SI Text S2, and Figure 6A).

Supplementary Figure S2 – Alpha values from steered molecular dynamics simulations

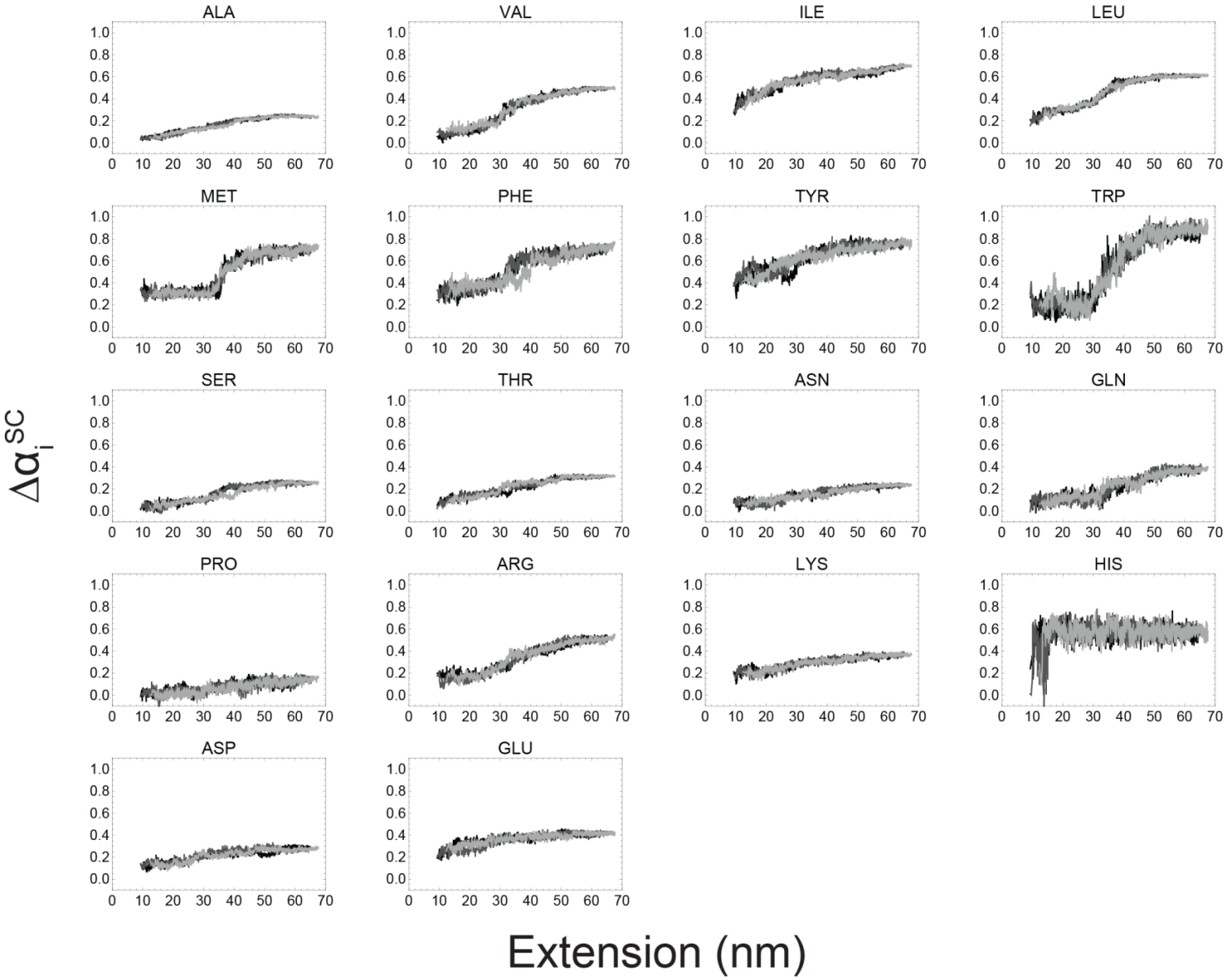

Supplementary Figure S2 – Shown are the calculated Δα values for all amino acids in T4* from the steered molecular dynamics simulations. These values are for the side chains (SC) and all three simulations are overlaid showing excellent reproducibility. Note that the majority of amino acids are simply a line between the initial Δα from the crystal structure to the maximum accessibility when fully extended. Average values corresponding to the dimensions of the unfolded state from the BHMM were used in transfer free energy calculations of the intermediate (SI Text S2, and Figure 6A).